J Mol Model (2008) 14:201–213
DOI 10.1007/s00894-007-0261-0

ORIGINAL PAPER

Electrostatic interactions play an essential role in DNA repair and cold-adaptation of Uracil DNA glycosylase

Magne Olufsen · Arne O. Smalås · Bjørn O. Brandsdal

Received: 22 August 2007 / Accepted: 3 December 2007 / Published online: 15 January 2008

Abstract Life has adapted to most environments on earth, including low and high temperature niches. The increased catalytic efficiency and thermoliability observed for enzymes from organisms living in constantly cold regions when compared to their mesophilic and thermophilic cousins are poorly understood at the molecular level. Uracil DNA glycosylase (UNG) from cod (cUNG) catalyzes removal of uracil from DNA with an increased k_{cat} and reduced K_m relative to its warm-active human (hUNG) counterpart. Specific issues related to DNA repair and substrate binding/recognition (K_m) are here investigated by continuum electrostatics calculations, MD simulations and free energy calculations. Continuum electrostatic calculations reveal that cUNG has surface potentials that are more complementary to the DNA potential at and around the catalytic site when compared to hUNG, indicating improved substrate binding. Comparative MD simulations combined with free energy calculations using the molecular mechanics-Poisson Boltzmann surface area (MM-PBSA) method show that large opposing energies are involved when forming the enzyme-substrate complexes. Furthermore, the binding free energies obtained reveal that the Michaelis-Menten complex is more stable for cUNG, primarily due to enhanced electrostatic properties, suggesting that energetic fine-tuning of electrostatics can be utilized for enzymatic temperature adaptation. Energy decomposition pinpoints the residual determinants responsible for this adaptation.

M. Olufsen · A. O. Smalås · B. O. Brandsdal (✉)
The Norwegian Structural Biology Centre,
Department of Chemistry, University of Tromsø,
N-9037 Tromsø, Norway
e-mail: Bjorn-Olav.Brandsdal@chem.uit.no

Keywords Continuum electrostatics · Free energy calculations · Molecular simulations · Protein-DNA binding · Uracil DNA glycosylase

Introduction

Organisms capable of survival in low temperature niches have been known for a long time, and are collectively referred to as psychrophilic (cold-loving). Most of our planet is covered with permanently cold regions, and life has effectively colonized most ecological niches. Survival in extreme environments requires that the organisms adapt their metabolisms to low temperature, including their enzymes. Mechanisms of enzymatic adaptation to cold environments are not presently well understood. Hochachka and Somero [1] suggested that organisms adapted to cold environments need to compensate the reduced temperature by expressing enzymes with increased flexibility to maintain a high catalytic efficiency. More recent investigations suggest that the increased catalytic efficiency of cold-adapted enzymes is not necessarily attributed to an overall increase in structural flexibility but rather to the key components directly involved in the catalytic cycle [2, 3]. Crystallographic analysis of uracil DNA glycosylase from cod (cUNG) and human (hUNG) did not provide indications of any differences in molecular flexibility [4]. Subsequent MD simulations indicated increased flexibility for the DNA binding loop in cUNG as compared to hUNG [5]. Structural analysis of psychrophilic and mesophilic trypsin did not reveal significant differences in overall flexibility [6], which was also supported by investigations using computer simulations [7]. However, both the crystallographic and the computational study of cold- and warm-active trypsin point towards different dynamic behavior in

localized regions as a possible mean for enzymatic adaptation to cold environments. Increased molecular flexibility is not necessarily the only strategy for adaptation to low temperature.

Alteration of the electrostatic potential of key residues has been proposed to play a central role in adaptation of citrate synthase [8]. Psychrophilic citrate synthase has significantly different electrostatic potentials at and around the active site in comparison to its thermophilic counterpart, and focused electrostatic attraction of substrates has been proposed to be a possible source for the enhanced catalytic activity of the cold-active citrate synthase [8]. Kumar and Nussinov [9] also found that electrostatics play different roles in psychrophilic and thermophilic citrate synthase. Qualitative investigations of the electrostatic surface potentials in seven trypsin isoenzymes using continuum electrostatic calculations showed a more negatively charged substrate binding site in the cold-adapted trypsin when compared to warm-active homologues [10]. Accommodation of small synthetic inhibitors and cognate amino acid side-chains to the specificity pocket of trypsin is electrostatically more favorable in the cold-adapted enzyme [11], suggesting that electrostatics is important in temperature adaptation. Optimization of electrostatics has also been suggested to be an adaptational strategy followed by cod UNG [4, 12].

Uracil DNA glycosylase is a DNA repair enzyme and is the first enzyme in the base excision repair pathway [13]. The enzyme catalyzes removal of uracil from single- and double-stranded DNA by cleaving the N-glycosylic bond between the target base and deoxyribose [14]. The crystal structure of the catalytic domain of the family 1 UNG from several species are known: human [15], cod [4], herpes simplex virus type-1 [16], *Escherichia coli* [17] and Epstein-barr virus [18]. Several crystal structures of hUNG and herpes simplex virus type-1 UNG in complex with DNA have also been determined [16, 19–22]. The catalytic domain of cUNG and hUNG consists of 223 residues, and the sequence identity between them is 75%. The overall topology is a typical α/β protein [15]. The four important loops for detection and catalysis are: the 4-Pro loop (^{165}PPPPS^{169}), the Gly-Ser loop (^{246}GS^{247}), the Leu272 loop (^{268}HPSPLSVYR^{276}) and the water-activating loop (^{145}DPYH^{148}) [20]. These loops are conserved between cUNG and hUNG. The amino acids mentioned above are from hUNG, and there are two substitutions in the Leu272 loop in the cUNG sequence: V274A and Y275H. The Leu272 loop is particularly important as it moves into the minor groove of the double-stranded DNA and is involved in the flipping of the uracil base. This movement is essential for bringing the catalytic important residue His268 within hydrogen bonding distance of the oxygen atom (O2) of uracil [20]. Even if the cold-adapted cUNG and the warm-adapted hUNG enzymes have very similar 3D structure, the cUNG enzyme is up to 10 times more catalytic efficient (k_{cat}/K_m) in the temperature range from 15–37 °C compared to the human homologue [23]. This is achieved through optimization of both kinetic parameters as k_{cat} is increased and K_m is reduced for cUNG. K_m is most affected and possibly reflects increased substrate interactions in the reaction catalyzed by the cold-adapted enzyme.

Enzyme-substrate interactions and the apparently improved substrate accommodations for cUNG are further explored using a range of computational techniques, including continuum electrostatics calculations, MD simulations and free energy calculations. We find that formation of the Michaelis-Menten complexes is highly favorable for both enzymes, but the cUNG-DNA complex is energetically more stable when compared to hUNG-DNA. Overall, this is attributed to improved electrostatic properties of cUNG, but also superior interactions between key structural areas and the substrate in the cold-adapted enzyme. The present investigations thus point to improved electrostatics as a possible route for cold-adaptation and enhanced catalytic efficiency.

Method

Structural models

Crystal structures were available for cUNG [4], hUNG [15] and hUNG-DNA [21]. The cUNG-DNA complex was modeled with the hUNG-DNA structure as template. This DNA had originally a 2′-deoxy-pseudouridine-5′monophosphate, but this base was modeled into a 2′-deoxy-uracil-5′ monophosphate by switching place for the atoms: C2 ↔ C4, O2 ↔ O4 and N1 ↔ C5, (Fig. 1). The latter is the uracil base, recognized and removed from the DNA by UNG. The double-stranded DNA from the crystal structure of hUNG-DNA consists of 19 bases. These structures were used as

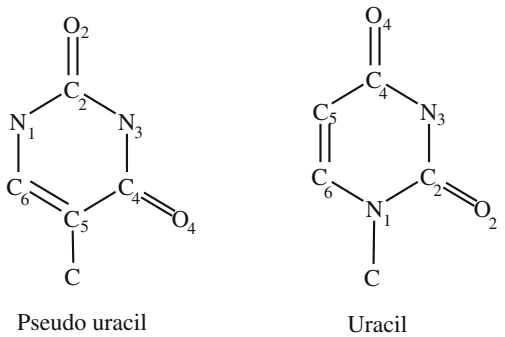

Pseudo uracil Uracil

Fig. 1 Structural differences between uracil and pseudo uracil

starting structures for the MD simulations. All the crystal structures were of the recombinant enzymes with three mutations in the N-terminal end: P82M, V83E and G84F. UNG contains several histidines, all except His148 were considered as neutral, and protonated at the Nε2 atom, in the simulations. These choices were based on data from NMR and continuum electrostatics calculations [24].

Molecular dynamics simulations

The AMBER9 program package [25] with the parm99 force field [26] was used to run and analyze the MD simulations. Water molecules were added to the protein with a 15 Å buffer from the edge of the box and described according to the TIP3P model [27]. Prior to the MD simulations, the molecular systems were subjected to 200 cycles of energy minimization of the water with the protein fixed and then 200 cycles of minimization of the whole system. In the initial phase, the temperature of the system was slowly raised in steps to the final temperature of 300 K, followed by an equilibration period of 110 ps. The production phase of the simulations was carried out in the isothermal-isobaric ensemble (300 K and one atmosphere pressure). Pressure and temperature were maintained by the Berendsen coupling algorithm [28]. A 8 Å cutoff was used for non-bonded interactions and the Particle-Mesh-Ewald method [29] was used to handle long-range interactions beyond the cutoff. SHAKE [30] was applied to constrain covalent bonds involving all hydrogen atoms. A time step of 2 fs was employed. Coordinates were written to file every 20 ps during the production phase, and the simulations were carried out for 10 ns for both cUNG and hUNG. The density, total energy, temperature and root-mean-square deviation plotted *vs* time were used to investigate the stability of the simulations, and all four properties are stable throughout the simulations (results not shown).

MM-(GB)PBSA

The MM-PBSA method [31–33] was used to calculate the binding energy of the protein-DNA complex. The structural ensembles consisting of 500 conformations collected every 20 ps in the MD simulations were post-processed using the MM-PBSA method. This method estimates the free energy of each conformation according to:

$$G = H_{MM} + G_{sol} - TS_{Solute} \quad (1)$$

where H_{MM} is the total molecular mechanical energy in the gas phase. H_{MM} is further divided into several energy terms:

$$H_{MM} = H_{bond} + H_{angle} + H_{torsion} + H_{elec} + H_{vdW} \quad (2)$$

$$G_{sol} = G_{Pol} + G_{np} \quad (3)$$

$$G_{np} = \gamma \cdot SASA + b \quad (4)$$

where H_{bond}, H_{angel}, $H_{torsion}$, H_{elec} and H_{vdW} are the bond, angle, torsion, electrostatic and van deer Waals energies in Eq. 2, respectively. G_{sol} is the solvation free energy and can be divided into two terms according Eq. 3. G_{pol} is the electrostatic solvation free energy, and is normally calculated with the Poisson-Boltzmann method (PB) [34] or with the Generalized-Born (GB) method [35, 36]. G_{np} is the nonpolar solvation free energy and is calculated with Eq. 4. In Eq. 1, the T is the temperature and S is the solute entropy. There are different ways to calculate the entropy [37], and the solute entropy is estimated using normal mode analysis [38] as implemented in the AMBER program package. The solute entropy of each snapshot is calculated from the structure minimized in vacuum with a distance-dependent dielectric constant of 4r and the convergence criterion for the energy gradient was set to 0.1 kcal mol^{-1} $Å^{-1}$. Quasiharmonic analysis and normal mode analysis can be used to calculate solute entropies from simulations [38, 39]. One limitation with quasiharmonic analysis is to obtain converged energies for the conformational entropy. Conformational entropic studies of a β-heptapeptide did not even show convergence after 150 ns of simulation [40, 41]. The normal mode approach requires energy-minimization of the conformations prior to the entropy calculations, and artefactual conformational changes may be introduced during the energy-minimization process [42].

The electrostatic contribution to the solvation free energy was calculated with the PBSA program in AMBER [34] for the binding free energies and with the GB method [35, 36] for the decomposition of binding free energies. We have also calculated the solvation free energy contribution to the binding energy with the GB method, and since the GB and PB gave similar results only the results from the PB calculations are shown. The solute and solvent dielectric constants were set to 1 and 80 in all PB and GB calculations, and the ionic strength was set to zero. In both methods, the parameters used to calculate the non polar contribution to the solvation energy (γ and b) was set to 0.0072 kcal/$Å^2$ and 0.0 kcal mol^{-1}, respectively. These parameters have been developed to be used with the AMBER force field [43]. The lattice spacing was set to 2 grids/Å and a maximum of 1000 iterations were used for the PBSA calculations. The solvent-accessible-surface-area (SASA) was calculated with a probe radius of 1.4 Å both in the PB and GB methods. The molsurf program [44] and the LCPO method [45] was applied to calculate the SASA in the PBSA and GB methods, respectively. When computing

the contribution from individual residues to the free energy of binding, the surface area was computed by recursively approximating a sphere around an atom starting from an icosahedra.

The binding free energy was calculated according to the following equation:

$$\Delta G_{bind} = \langle G_{complex} \rangle - \langle G_{receptor} \rangle - \langle G_{ligand} \rangle \quad (5)$$

where $<G_{complex}>$, $<G_{receptor}>$ and $<G_{ligand}>$ are the average free energies of the protein-DNA complex, protein, and the DNA, respectively, using 500 MD structures.

Continuum electrostatics calculations and surface potentials

The DelPhi program [46, 47] was used to calculate the electrostatic potential of cUNG and hUNG. His148 was charged in the continuum electrostatics calculations, in addition to all Lys, Arg, Glu and Asp residues. The calculations were performed using the partial charges and atomic radii of the AMBER force field (parm99) [26]. The electrostatics was calculated using the linear Poisson-Boltzmann equation and a grid size of 165×165×165 points in a 3-dimensional grid. Stepwise focusing was used to increase the accuracy [48]. Initially a rough grid was calculated with the Coulombic boundary conditions. The resulting grid of this calculation was adopted as the boundary condition for two further focused calculations, and in the last calculation the molecule occupied ~85% of the box. A solvent probe of 1.4 Å was used to calculate the molecular surface. These calculations were run with zero ionic strength and the dielectric constants of the protein and the water were set to 20 and 80, respectively.

Results and discussion

Qualitative investigations - continuum electrostatic calculations

Enzymes need to form a complex with their substrates before they can exert their mode of action. Electrostatic interactions play a key role in virtually all biological systems, and are expected to be of particular importance for enzymes with DNA as substrate, as DNA is highly charged. Figure 2 shows the positive electrostatic isocontour extending out of the binding site, interacting favorably with the negative isocontour from the DNA strand. It has been proposed that the increased substrate affinity observed for cUNG when compared to hUNG is due to enhanced positive electrostatic potential at surface areas central to formation of the enzyme-substrate complex [4, 12]. The charge of the phosphodiesters on the target nucleotide and the two connected nucleotides has been shown to have a large effect on the ground state (K_m effects) value and an even greater effect on the ionic transition state (k_{cat}/K_m effects) [49]. It is thus reasonable to expect that altering the charges in the active site region will also affect binding of the DNA.

In Fig. 3, the electrostatic surface potentials and isocontours for cUNG and hUNG are presented, and both cUNG and hUNG have, as expected, highly positive electrostatic potentials in the specificity pocket and in nearby areas that are know to interact directly with DNA. Figures 3 a and b also reveal that the psychrophilic enzyme has more positive electrostatic potentials close to both terminals of the DNA fragment. Residue 171, which is Glu and Val in hUNG and cUNG respectively, is particularly interesting when it comes to possible differences in

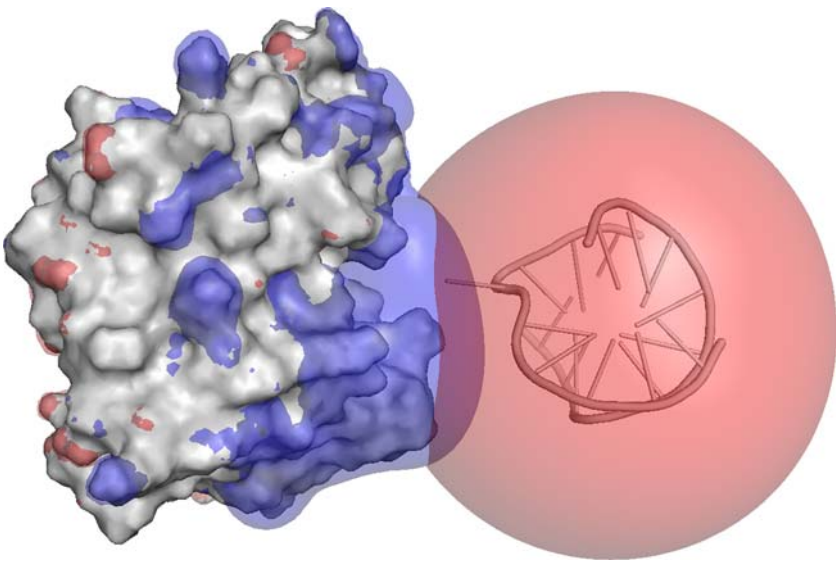

Fig. 2 Electrostatic isosurfaces of cUNG and DNA. The DNA was moved 15 Å out of the specificity pocket as observed in the model of cUNG-DNA. The isocontour surface of cUNG was set to −5 kT/e (red) and 5 kT/e (blue), while the isocontour surface of DNA was set to −3 kT/e (red) and 3 kT/e (blue) The figure was generated using PyMol [70]

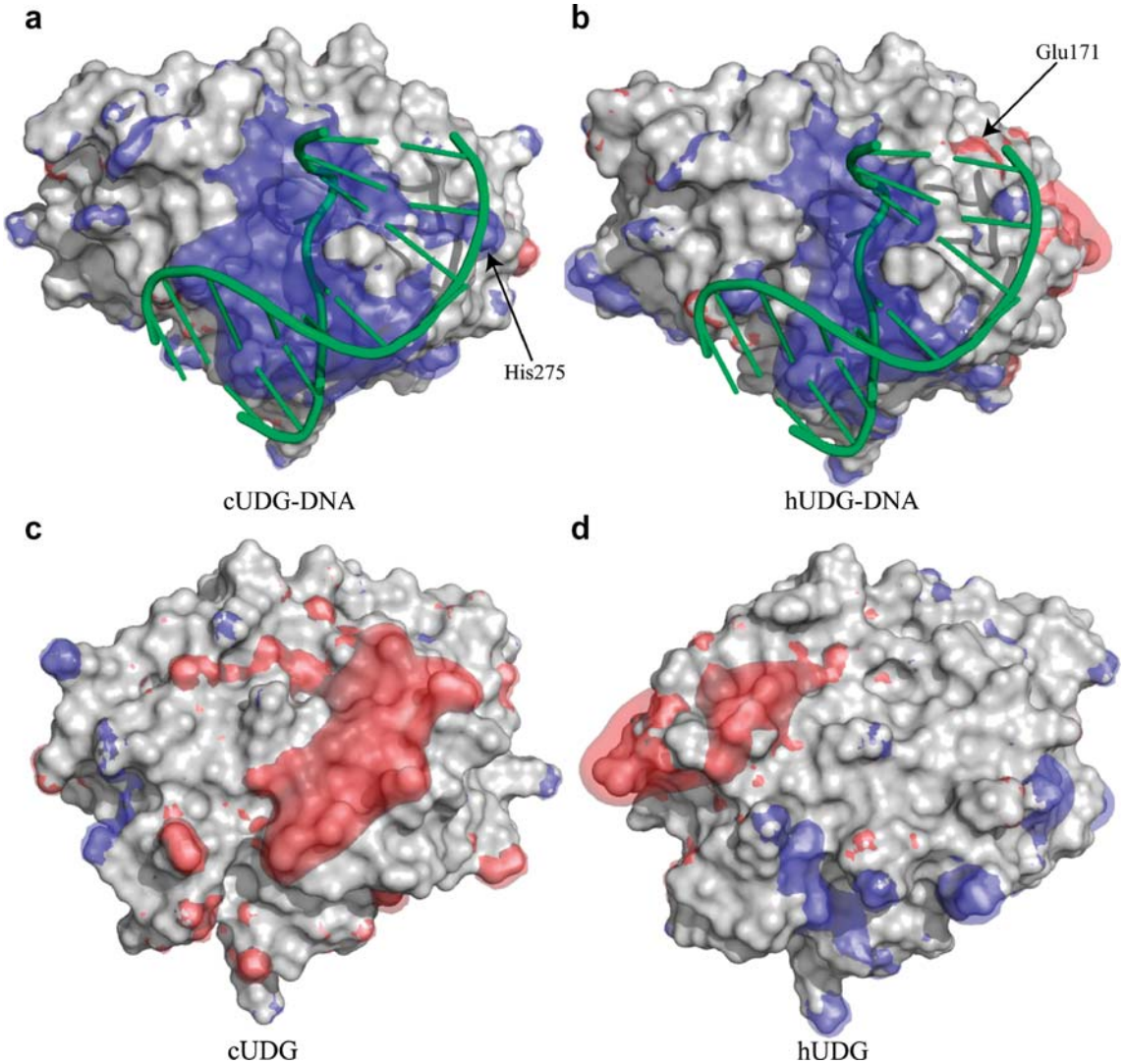

Fig. 3 Electrostatic isosurfaces of cUNG and hUNG. (**a**) and (**b**) show cUNG and hUNG bound to dsDNA, and (**c**) and (**d**) show cUNG and hUNG from the opposite side of the specificity pocket, respectively. The isocontour surfaces correspond to −2 kT/e (red) and 4 kT/e (blue). The figure was generated using PyMol [70]

substrate binding. hUNG and cUNG have K_m values of 2.4 μM and 0.8 μM at 295 K [12], respectively, corresponding to three times higher K_m for hUNG compared to cUNG. Mutations of residue 171 change the K_m value to 0.7 and 1.7 μM for hUNG-E171V and cUNG-V171E [12], respectively. Mutation of this residue thus yields a hUNG enzyme with similar K_m as the cUNG, but also visa versa. Since K_m is roughly an inverse measure of the binding strength between the enzyme and its substrate [50], lower K_m values indicate stronger association between the enzyme and substrate. Figures 3 a and b also show that there are larger areas with positive potential at the flanking sides of the catalytic site, suggesting stronger non-specific interactions between the cold-adapted enzyme and DNA. Ultimately, this can lead to increased stability of the UNG-DNA complex. Furthermore, the more positive electrostatic potential where the DNA strand interacts with the enzyme, will accommodate for a more efficient recognition of DNA and orient it in the correct position for catalytic cleavage.

It is also interesting to examine the potentials in other areas of the structures, and particularly at the opposite side of the DNA binding site. Both enzymes have predominantly negative electrostatic surface potentials here, but cUNG possesses a larger area with negative electrostatic potential when compared to its warm-active homologue (Figs. 3 c and d).

Thermodynamic analysis of UNG-DNA interactions

Qualitative examination of the electrostatic properties of cUNG and hUNG (Fig. 3) encouraged us to initiate more accurate investigations of the enzyme-substrate complexes

using free energy calculations with conformational sampling. There are currently few computational methods that allow for the determination of binding energies between protein and DNA. The estimation of the absolute free energy of binding was carried out using the MM-PBSA approach, which was initially used to study the stability of various DNA and RNA fragments [33]. In later years, however, the method has also been applied to calculate binding free energies of proteins and small ligand [51, 52], protein-protein [53–55], protein-RNA [56] and protein-DNA [57]. It is challenging to calculate the absolute binding energy for association of highly charged large macromolecules, but the MM-PBSA method has proven to be able to qualitatively reproduce the absolute binding energies for such systems [56]. The binding free energy can be calculated in two ways with the MM-PBSA method, either using a single MD simulation of the complex or using individual simulations of complex, protein and ligand. The former is referred to as the single trajectory MM-PBSA method whereas the latter is referred to as the multiple trajectories MM-PBSA. The single trajectory approach assumes that there are no conformational changes in the protein or in the ligand from the unbound to the bound state, which may in some cases, be a rather drastic assumption. Successful application of both single and multi trajectory calculations have been reported [56, 58]. Here, results from both protocols are reported.

Free energies of binding - stability of the enzyme substrate complexes

The individual contributions and the resulting free energies of formation of the Michaels-Menten complex for cUNG and hUNG are presented in Tables 1 and 2, respectively. The data presented show that relative difference in stability of the two complexes are −5.6 kcal mol^{-1} and −3.4 kcal mol^{-1} in favor of cUNG when using single and multiple trajectories, respectively, indicating improved interactions in the complex with the cold-adapted enzyme. Tables 1 and 2 show that the enthalpies of binding are very favorable in all four cases, while the binding entropies oppose binding. The contribution from the solute entropy to the binding free energy varies in the two methods, but is of similar magnitude. Estimation of the entropy is perhaps the most challenging part of calculating binding energies, due to changes in the degree of freedom of the solutes [58]. The change in solvent entropy upon binding is not explicitly included in the MM-PBSA method, but included implicitly in the change in SASA associated with binding [56]. The rotational and translational contribution to the entropy is identical for both the single and separate trajectory method and also identical for the two enzymes. Thus, the difference observed in ΔS between the two enzymes is caused by the vibrational part of the entropy. Cold-adapted enzymes are thought to have increased molecular flexibility, and

Table 1 Binding free energies of the cUNG-DNA complex*,† computed with MM-PBSA from single and multiple trajectories

Contribution‡	cUNG-DNA	cUNG	DNA	Delta¶
H_{elec}(single)	−7913.8±4.1	−6118.4±3.5	350.7±1.7	−2146.1±3.3
H_{vdW}(single)	−1235.2±1.2	−1012.4±1.1	−133.5±0.4	−89.3±0.3
H_{int}(single)	5618.7±2.0	4745.2±1.9	873.5±0.8	0.0±0.0
G_{np}(single)	95.8±0.1	76.7±0.1	30.0±0.1	−10.9±0.1
G_{pol}(single)	−4683.2±3.6	−2615.7±3.2	−4221.3±1.5	2153.8±3.3
$G_{gas+solv}$(single)	−8117.7±2.3	−4924.6±2.0	−3100.6±0.8	−92.5±0.4
TS_{tot}(single)	2955.1±0.7	2498.6±0.6	509.2±0.3	−52.7±0.9
G_{tot}(single)	−11072.8±2.4	−7423.2±2.1	−3609.8±0.8	−39.8±1.0
H_{elec}(multi)	−7913.8±4.1	−6081.7±3.3	355.4±2.0	−2187.5±5.5
H_{vdw}(multi)	−1235.2±1.2	−1001.8±1.2	−139.9±0.4	−93.5±1.8
H_{int}(multi)	5618.7±2.0	4731.6±2.0	871.6±0.8	15.5±2.9
G_{np}(multi)	95.8±0.1	79.1±0.1	29.7±0.1	−13.0±0.1
G_{pol}(multi)	−4683.2±3.6	−2650.6±3.3	−4224.6±1.9	2192.0±5.1
$G_{gas+solv}$(multi)	−8117.7±2.3	−4923.4±2.0	−3107.8±0.8	−86.5±2.9
TS_{tot}(multi)	2955.1±0.7	2504.8±0.6	508.2±0.2	−57.9±1.0
G_{tot}(multi)	−11072.8±2.4	−7428.2±2.1	−3616.0±0.8	−28.7±3.1

*All values are given in kcal mol^{-1}.

†Mean value calculated using 500 snapshots reported with standard error of the mean, which is obtained by dividing the standard deviation by the square-root of the number of snapshots (500).

‡H_{elec}: Coulombic energy, H_{vdW}: van der Waals energy, H_{int}: internal energy, G_{np}: nonpolar solvation free energy, G_{pol}: polar solvation free energy, $G_{gas+solv} = H_{elec} + H_{vdW} + H_{int} + G_{np} + G_{pol}$, TS_{tot}: total entropy contribution, $G_{tot} = G_{gas+solv} + TS_{tot}$.

¶Delta = (UNG-DNA) - (UNG) - (DNA)

Table 2 Binding free energies for the hUNG-DNA complex*,† computed with MM-PBSA from single and multiple trajectories

Contribution[c]	hUNG-DNA	hUNG	DNA	Delta[d]
H_{elec}(single)	−7452.0±3.8	−5838.8±3.4	325.8±1.7	−1939.0±2.9
H_{vdW}(single)	−1241.1±1.1	−1014.7±1.1	−130.0±0.4	−96.4±0.3
H_{int}(single)	5671.7±2.1	4796.2±1.9	875.5±0.8	0.0±0.0
G_{np}(single)	98.3±0.1	80.0±0.1	30.4±0.1	−12.1±0.1
G_{pol}(single)	−4880.2±3.3	−2630.8±2.9	−4203.9±1.6	1954.5±3.0
$G_{gas+solv}$(single)	−7803.3±2.1	−4608.1±1.9	−3102.2±0.8	−92.7±0.5
TS_{tot}(single)	2981.6±0.8	2527.8±0.6	512.2±0.3	−58.4±1.0
G_{tot}(single)	−10784.9±2.3	−7136.2±2.0	−3614.4±0.8	−34.3±1.1
H_{elec}(multi)	−7452.0±3.8	−5804.0±3.6	355.4±2.0	−2003.4±5.9
H_{vdw}(multi)	−1241.1±1.1	−1009.0±1.1	−139.9±0.4	−92.2±1.6
H_{int}(multi)	5671.7±2.1	4802.3±1.9	871.6±0.8	−2.2±2.9
G_{np}(multi)	98.3±0.1	81.1±0.1	29.7±0.1	−12.5±0.1
G_{pol}(multi)	−4880.2±3.3	−2685.4±3.5	−4224.6±1.9	2029.8±5.3
$G_{gas+solv}$(multi)	−7803.3±2.1	−4615.0±2.0	−3107.8±0.8	−80.5±3.0
TS_{tot}(multi)	2981.6±0.8	2528.6±0.7	508.2±0.2	−55.2±1.0
G_{tot}(multi)	−10784.9±2.3	−7143.6±2.1	−3616.0±0.8	−25.3±3.2

*All values are given in kcal mol^{-1}.
†Mean value calculated using 500 snapshots reported with standard error of the mean, which is obtained by dividing the standard deviation by the square-root of the number of snapshots (500).
‡H_{elec}: Coulombic energy, H_{vdW}: van der Waals energy, H_{int}: internal energy, G_{np}: nonpolar solvation free energy, G_{pol}: polar solvation free energy, $G_{gas+solv} = H_{elec} + H_{vdW} + H_{int} + G_{np} + G_{pol}$, TS_{tot}: total entropy contribution, $G_{tot} = G_{gas+solv} + TS_{tot}$.
¶Delta = (UNG-DNA) - (UNG) - (DNA)

psychrophilic UNG has been shown to possess a more flexible DNA recognition loop compared to mesophilic hUNG [4, 5, 12]. One should then expect that the cold-adapted cUNG would show the largest difference in entropy upon binding, and this is actually the case in the separate trajectory method (Tables 1 and 2). In the single trajectory method, on the other hand, the opposite is observed, as the mesophilic enzyme show the largest loss in entropy upon binding. It should be noted that the single trajectory results do not take conformational changes occurring upon binding into account. The conformations for the unbound state in the single trajectory method are extracted from the simulation of the complex, which explain why the cold-adapted enzyme does not possess a larger loss in entropy with the single trajectory method.

Kinetic experiments have shown that cUNG associates more favorably to DNA compared to its warm-active homologue hUNG (reduced K_m), as discussed previously. When examining the different contributions to the binding free energy, it is interesting to note that the electrostatic contribution to the free energy of binding is much more negative (favorable) for the psychrophilic UNG as compared to its warm active homologue (Tables 1 and 2). The continuum electrostatics calculations showed that cUNG has a more positive electrostatic surface potential near the active site (Fig. 3). It thus seems reasonable that this enzyme will have more favorable electrostatic interactions with the negatively charged DNA.

Whether the free energies of binding can be computed from the simulation of only the complex, depend upon the structural changes which the protein and DNA undergo during complex formation. Crystal structures are available of both cUNG and hUNG without DNA present, but structure of the complex with DNA is only available for hUNG. Nonetheless, comparison of hUNG with and without DNA bound reveal that there are only minor conformational differences between bound and unbound enzyme. The overall backbone root-mean-squared deviation (r.m.s.d.) between the two structures is 1.43 Å. No experimental structure is, however, available for examination of possible changes in the DNA strand during the binding process. DNA is not a static structure but undergoes rapid unpairing of individual base pairs and slow large cooperative unfolding events [59, 60]. There is an ongoing debate on how DNA repair enzymes, such as DNA glycosylases, recognize rare damaged bases in a large background of normal DNA bases. Two views for localization of damaged sites have emerged: the *base sampling model* and the *inherent extrahelicity model*. The *base sampling model* suggests that UNG localizes uracil by breaking base pairs and flip them out to test them against the interactions offered in the specificity pocket [61]. In the *inherent extrahelicity model*, the base pairs involving uracil is inherently weak and uracil will spontaneous flip out to an extrahelical conformation, complementary to the binding interactions offered by UNG [59, 61]. NMR imino proton experiments have also

shown that the U·A base pairs rapidly open at room temperature and the opening rates are greater or equal to the rate constants for the kinetic steps of base flipping of UNG [59, 62]. It has been shown that UNG does not alter the opening rate of the base but instead slows the closing rate of the A·U base pair [59]. Irrespective of how the enzyme actually localizes the damaged base, the Michealis-Menton complex will be the same for the two proposed mechanisms.

The structure of DNA when bound to hUNG indicates distortions from ideal geometry as the DNA strand is bent. As has been pointed out by others [62], the energetic effect of DNA bending is highly unfavorable and constitutes a significant contribution to enzymatic base flipping. The energetic effect of DNA bending is very challenging to capture, and is not fully accounted for in our free energy calculations. If the *base sampling model* is correct, an additional contribution is missing, corresponding to the free energy required to break the base pair and flip the base into the active site of the enzyme. Thus, neglect of the contribution from DNA bending and possibly flipping of the damaged base will lead to an overestimation of the stability of the Michaelis-Menten complexes. The initial model for the simulations of unbound DNA was constructed from the DNA observed in the crystal structure of hUNG-DNA (1EMH [21]). Both the uracil and the pairing partner adenine are flipped out in an extrahelical conformation in the starting structure. In the MD simulation of unbound DNA, the adenine base which pairs to uracil flips back into the DNA helix, but the uracil base does not. However, the lifetime of an extrahelical base is between 100–800 ns [63] and the present simulations times are 10 ns, thus probably too short a time to observe spontaneous base flipping. The DNA structure bound to hUNG is bent to the enzyme surface causing the flanking phosphate bases to be compressed, as judged by the distance between the phosphorus atoms at the nucleotides connected to the uracil nucleotide is compressed from ~12 to 7.7 Å [20, 21]. The distance between the same phosphorus atoms is 11.9 Å in the final structure of the simulation of free DNA, showing that the DNA bends back into its favorable relaxed orientation.

The results presented in Tables 1 and 2 can actually be used to examine the energetic penalty arising from bending of DNA. Because the strain in the DNA when it is bound to UNG is released in the simulation of unbound DNA, the differences between these energies and those for DNA when bound correspond to the bending energy. This contribution is 6.2 kcal mol^{-1} and 1.6 kcal mol^{-1} for cUNG and hUNG, respectively. Experimentally, the energetic cost with DNA bending for hUNG has been estimated to be between 3 and 4 kcal mol^{-1} [62]. Hence, our simulations provide a good estimate of this energy contribution, and the larger penalty observed for cUNG probably reflects the increased K_m.

Statistical considerations

The standard deviations for the values reported in Tables 1 and 2, obtained by multiplying them with $\sqrt{500}$, are up to three times higher than the mean values. Others have also observed large standard deviations for protein-DNA calculations using the MM-PBSA methodology [57]. We emphasize that the standard deviation is not a measure on the error inherent in the determined averages, but rather a measure of the variation throughout the sample. The free energies of protein-DNA complexes are on the order of several thousands kcal mol^{-1}, making the determination of absolute binding free energies challenging as we are subtracting large numbers to obtain a small number. When we plot the sum of the gas-phase energies and the solvation free energy for cUNG and hUNG extracted from multiple simulations, stable energies with fluctuations within 4 % of the mean values are observed (Fig. 4). Another way of evaluating the stability (or convergence) of the computed free energies is to compare the energetics for the first and second half of the trajectories (Table 3), and use these as upper and lower limits for the intrinsic error. The binding energies from the first and second half of the simulations are very similar, yielding virtually identical error as the standard error of the mean reported in Tables 1 and 2. Thus, we can conclude that the MD simulations and the free energies extracted are stable.

Determinants of binding - decomposition of the binding free energy

One of the advantages of computer simulations over experiments is the possibility to perform decomposition of the free energies into residual contributions. Residual contributions are presented in Fig. 5. Figure 5 shows that the binding free energy per residue varies from −9.0 kcal mol^{-1} to +2.6 kcal mol^{-1}. Examining Fig. 5 immediately shows that the four loop regions which have been suggested to be important for detection and catalysis, emerge as the areas with the most favorable contribution to the binding free energy: the 4-Pro loop (^{165}PPPPS^{169}), the Gly-Ser loop (^{246}GS^{247}), the Leu272 loop (^{268}HPSPLSVYR^{276}) and the water-activating loop (^{145}DPYH^{148}). The four loops contribute with −74.7 kcal mol^{-1} and −73.7 for hUNG-DNA and cUNG-DNA, and are thus responsibly for 66.2 % and 70.4 % of the enthalpic contribution to the binding free energy in hUNG and cUNG, respectively.

The catalytically important residue, Asp145, located in the water-activating loop, is believed to form unfavorable interactions with the 3′-phosphodiester group of the

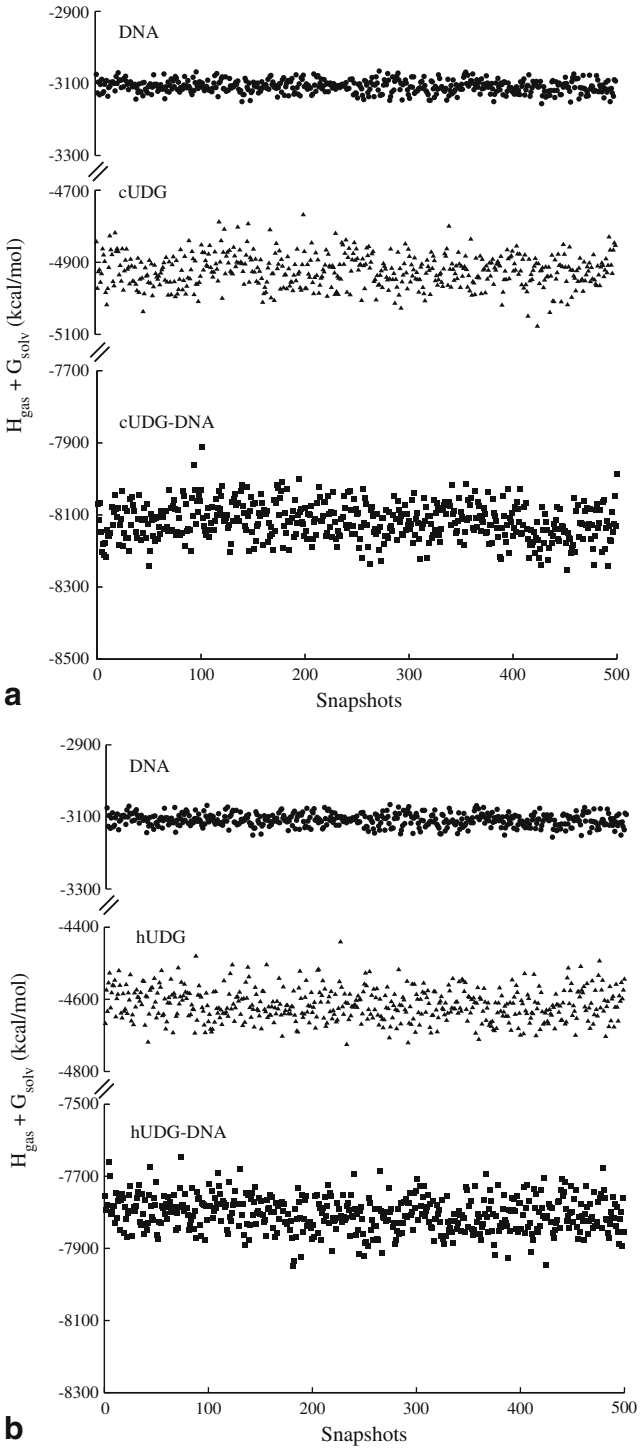

Fig. 4 Sum of energies from gas phase and solvation free energies calculated for 500 snapshots of the cUNG-DNA (**a**) and hUNG-DNA (**b**) complex. The solvation free energies were calculated with the PB method. The snapshots were taken from separate trajectories. The circles, triangles and the squares represent DNA, UNG and UNG-DNA complex, respectively

Table 3 Binding free energies* calculated for the first† and second‡ half of the UNG-DNA simulations and their contributions

Enzyme	Contributions¶	First half	Second half
cUNG	ΔH_{gas}	−2231.3±8.2	−2299.7±8.3
cUNG	ΔG_{sol}	2148.2±6.6	2210.3±7.2
cUNG	$T\Delta S_{tot}$	−57.4±1.3	−58.3±1.4
cUNG	ΔG_{tot}	−25.6±4.4	−31.1±4.3
hUNG	ΔH_{gas}	−2071.5±9.8	−2124.3±8.1
hUNG	ΔG_{sol}	1991.4±8.2	2043.8±6.2
hUNG	$T\Delta S_{tot}$	56.2±1.5	54.1±1.5
hUNG	ΔG_{tot}	−23.9±4.5	−26.4±4.6

*All values are given in kcal mol^{-1}.
†Mean value calculated using 250 snapshots with standard error of the mean.
‡First half includes snapshots 1–250, while second half includes snapshots 251–500.
¶ΔH_{gas}: gas phase energy, ΔG_{sol}: solvation free energy, $T\Delta S_{tot}$: total entropy contribution, ΔG_{tot}: $\Delta H_{gas} + \Delta G_{sol} - T\Delta S_{tot}$.

deoxyuridine residue of the substrate [64]. This view is supported by our calculations, as Asp145 has the most positive interaction free energy of all residues, +2.3 kcal mol^{-1} and +2.6 kcal mol^{-1} in cUNG and hUNG, respectively (Fig. 5).

The Leu272 loop or the DNA recognition loop plays an important role in uracil recognition and penetrates into the minor grove of the dsDNA in the complex [65, 66]. The Leu272 loop is also believed to play a role in flipping of the uracil base, either to flip out the uracil base from the DNA helix or to work as a "doorstop" to prevent the already flipped-out uracil to flip back into the dsDNA helix [65, 66]. The Leu272 loop interacts strongly with DNA in both enzymes and is responsible for 34.1 % and 44.2 % of

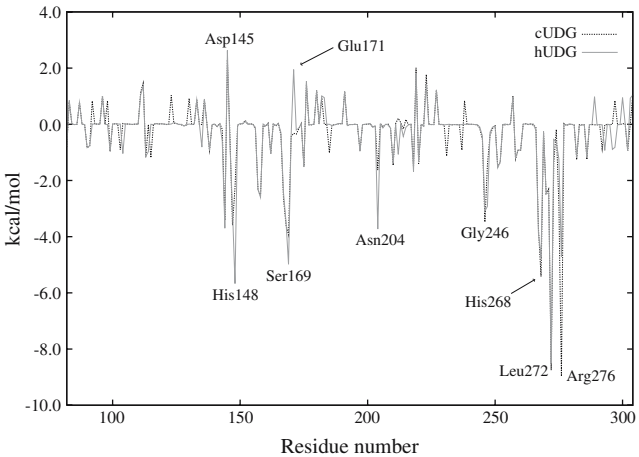

Fig. 5 Free energy of binding per residue of cUNG (black dashed line) and hUNG (gray) in complex with DNA with important residues highlighted

Table 4 Contributions* to the free energy of binding†,‡ from residues in the Leu272 loop in hUNG

Residue	ΔH_{elec}	ΔH_{vdW}	ΔG_{pol}	ΔG_{np}	$\Delta G_{gas+sol}$
His268	−1.5	−3.1	0.1	−0.2	−4.7
Pro269	1.8	−0.5	−1.6	0.0	−0.3
Ser270	−7.2	−2.3	7.3	−0.2	−2.5
Pro271	−0.3	−3.3	1.5	−0.4	−2.4
Leu272	−0.2	−7.9	0.6	−1.1	−8.5
Ser273	−2.8	−1.9	4.4	−0.2	−0.5
Val274	−3.1	−0.4	2.9	0.0	−0.6
Tyr275	−4.0	−2.8	6.1	−0.5	−1.2
Arg276	−219.9	−3.5	219.4	−0.7	−4.7
Sum	−237.2	−25.7	240.6	−3.3	−25.5
Average	−26.4	−2.9	26.7	−0.4	−2.8

*H_{elec}: Coulombic energy, H_{vdW}: van der Waals energy, G_{np}: nonpolar solvation free energy, G_{pol}: polar solvation free energy, $G_{gas+solv} = H_{elec} + H_{vdW} + H_{int} + G_{np} + G_{pol}$.
†Mean values calculated using 500 snapshots are reported, and the standard error of the $DG_{gas+sol}$ are ± 0.1 kcal mol^{-1}.
‡Mean value calculated from 500 snapshots with standard error of the mean of ± 0.1 kcal mol^{-1} for the ΔG_{tot}.

the enthalpic contribution to the binding energy in the warm-active and cold-adapted UNG, respectively. Tables 4 and 5 show the contributions to the binding free energy from each residue in the Leu272 loop for the two enzyme homologues. Three residues interact very favorably with DNA: His 268, Leu272 and Arg276. The largest differences in the interaction free energy per residue between the cold- and the warm-active enzyme are observed in this loop. Arg276 contributes with -4.7 kcal mol^{-1} in hUNG and −9.0 kcal mol^{-1} in cUNG to their respective free energies of binding. The side chain of Arg276 is closer to the DNA fragment in cUNG than in hUNG, and is within hydrogen bonding distance (3.40 Å) of two different DNA bases in cUNG (Fig. 6). Arg276 is in contrast not within hydrogen bonding distance of DNA in hUNG. This difference between the Arg276 in cUNG and hUNG can probably be explained by residue 275, which is Tyr in hUNG and His in cUNG. While the hydrophobic Tyr side chain points away from the DNA, the His275 side chain forms a hydrogen bond to O5′ atom on the adenine base opposite of the uracil base. The DNA strand is pulled closer to the enzyme in the simulation of cUNG because of this. The remaining residues in the Leu272 loop of cUNG form similar hydrogen bonds as described for the hUNG-DNA complex [22].

Table 5 Contributions* to the free energy of binding†,‡ from residues in the Leu272 loop in cUNG

Residue	ΔH_{elec}	ΔH_{vdW}	ΔG_{pol}	ΔG_{np}	$\Delta G_{gas+sol}$
His268	−4.1	−2.9	1.8	−0.2	−5.4
Pro269	1.2	−0.4	−1.0	0.0	−0.3
Ser270	−6.5	−2.4	6.6	−0.2	−2.5
Pro271	0.0	−2.7	0.7	−0.3	−2.3
Leu272	0.7	−7.6	−0.9	−1.0	−8.8
Ser273	−4.3	−1.6	4.8	−0.2	−1.4
Ala274	−3.1	−0.2	3.1	0.0	−0.2
His275	−13.0	−1.7	12.2	−0.3	−2.9
Arg276	−237.7	−2.1	231.4	−0.6	−9.0
Sum	−266.8	−21.7	258.6	−2.7	−32.6
Average	−29.6	−2.4	28.7	−0.3	−3.6

*H_{elec}: Coulombic energy, H_{vdW}: van der Waals energy, G_{np}: nonpolar solvation free energy, G_{pol}: polar solvation free energy, $G_{gas+solv} = H_{elec} + H_{vdW} + H_{int} + G_{np} + G_{pol}$.
†All values are given in kcal mol^{-1}.
‡Mean values calculated using 500 snapshots are reported, and the standard error of the $DG_{gas+sol}$ are ± 0.1 kcal mol^{-1}.

The Leu272 residue which penetrates into the minor grove of the dsDNA has a strong contribution to the binding free energy, which is dominated by hydrophobic or non-polar interactions (van der Waals term in Tables 4 and 5). Mutation of Leu272 to Ala has a large effect on the catalytic efficiency when single stranded DNA is used as substrate [66]. For the single stranded DNA the Leu272 loop does not need to flip out the uracil or work as a "doorstop" as in dsDNA. This indicates that Leu272 may also have another task in the catalytic mechanisms. The highly favorable binding energy of the Leu272 residue is important for stabilization of the enzyme-DNA complex, and might be important to orient the DNA in the right position for catalytic cleavage. Our calculations also add further support to this. Mutational studies have shown that His268, Ser270, Leu272 and Arg276 are all critical for hUNG activity [67], which may according to the presented energy decomposition, be a result of their favorable interactions with DNA. Thus, it seems likely that a strong binding between UNG and DNA is important in order to achieve a high catalytic activity. His275 in cUNG interacts more strongly with DNA when compared to the Tyr275 in hUNG. However, the cUNG-H275Y mutant shows no significant difference in K_m compared to cUNG, but the mutant has a reduction in catalytic efficiency caused by a reduced k_{cat} [12]. One explanation for this could be that the His275 residue binds stronger to the transition state than to the ground state, affecting k_{cat} instead of K_m. His275 is also thought to be the main contributor to the increased flexibility of the DNA recognition loop in the cold-adapted cUNG [5].

The continuum electrostatics investigation (Fig. 3) showed that the substitution of Val171 in cUNG to Glu in hUNG yielded a large change in the electrostatic potential at the surface in the vicinity of the active site. Val171 has a small favorable contribution to the binding energy (−0.3 kcal mol^{-1}), while Glu171 has an unfavorable contribution of +2.0 kcal mol^{-1}, as expected. The distance

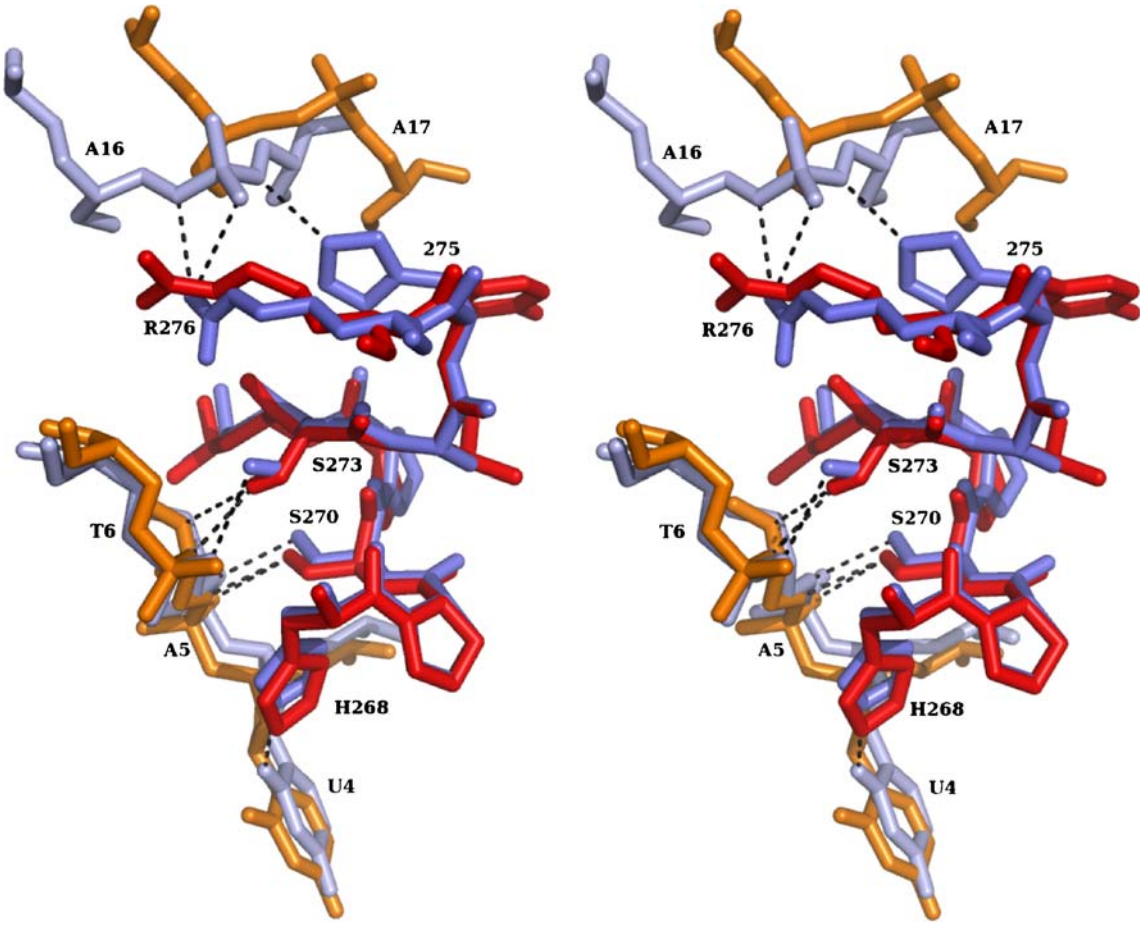

Fig. 6 Stereographic illustration of the interactions between the Leu272 loop and the DNA as observed in the MD simulations. Only the DNA nucleotides that interact with the Leu272 loop are shown for clarity. The bases are removed for all nucleotides except the uracil base. All residues in the Leu272 loop (residue 268–276) for both cUNG (blue) and hUNG (red) are shown. The DNA from the cUNG-DNA and the hUNG-DNA simulations are shown in light blue and orange, respectively. Only hydrogen bonds between UNG and DNA shorter than 3.4 Å are shown. The figure was generated in PyMol [70]

between the Glu171 Oε1 atom and the closest oxygen at the DNA terminal base is 8.43 Å in the crystal structure (1EMH [21]). The DNA fragment in this crystal structure consists of only 19 nucleotides, but if a longer DNA strand is used, this distance would decrease significantly, leading to more repulsive forces. Since K_m is related to the binding energy, it seems likely that the unfavorable binding energy for Glu171 could explain the observed difference in K_m value between cold- and warm active UNG. Hence, this residue could possibly be a key residue in the explanation of cold-adaptation in UNG.

Concluding remarks

Enzymes from organisms living at extreme temperatures need to maintain sufficient structural integrity to allow for catalytic efficiency, while at the same time avoid hot and cold denaturation. Uracil DNA glycosylase is a very good model system not only to study environmental adaptation of enzymes, but also to investigate the DNA repair process itself. Comparative investigations using different levels of theory have been applied to explain the increased catalytic efficiency of UNG from cod and human, and to gain a deeper insight into the DNA repair process. The results show that the stability of the Michealis-Menten complex is higher for cUNG when compared to hUNG, and is attributed to improved electrostatic properties on an overall level. Differences in key structural regions, vital to detection of damaged bases and the subsequent catalytic removal of uracil, between cold- and warm-active UNG were identified through decomposition of the free energy of binding into a residual level. This data is of significant interest to future engineering of the cUNG and hUNG enzymes, as it suggests residues important to not only catalysis but also substrate recognition.

Electrostatics is important for UNG in both substrate recognition/binding and catalysis. cUNG and hUNG are exposed to different environmental conditions, and thrive around 0–5 °C and 37 °C respectively. Temperature

influences properties of electrostatic origin in many ways, which are important to keep in mind when discussing enzymatic temperature adaptation. The most obvious effect comes from the changes in the dielectric constant of water, which is around 88 at 0 °C and decreases to about 55 when the temperature reaches the boiling point. Electrostatic interactions will thus become less screened as the temperature increases, and intuitively more favorable. Attractive electrostatic interactions are formed exothermically and stabilized at lower temperatures, in contrast to non-polar interactions that are destabilized at lower temperature, possibly counteracting the increased screening effect.

Estimation of the absolute binding free energy is in many cases a difficult task and is especially tricky when large interaction energies are involved. While the literature contains many examples of successful predictions of ΔG_{bind} for protein-small ligand complexes, few studies have been reported that estimate the stability of protein-DNA complexes, possibly due to the enormous challenge of obtaining accurate and precise estimates. There is presently no experimental association constants available for binding of the DNA fragment studied here to cUNG or hUNG. Experimental studies have, however, shown that hUNG binds to dsDNA containing uracil homologues with a binding strength of ~ −9.0 kcal mol^{-1} [67]. Other experimental bindings studies of *Escherichia coli* UNG bound to different DNA fragments show that the binding free energy varies from −8.0 kcal mol^{-1} to −15.0 kcal mol^{-1} [62, 68, 69]. The free energies presented here therefore appear to be overestimated with both procedures, but the relative difference between cUNG and hUNG is less sensitive to the choice of single *vs* multiple trajectories. The relative differences between cUNG and hUNG are in agreement with the increased substrate affinity observed for cUNG, particularly when the conformational change occurring during complex formation is taken into account (multiple trajectories). Further support to our calculations is added through the estimate of the energetic penalty associated with DNA bending, which is in agreement with experimental values, and the fact that all regions important to catalysis and substrate binding are pinpointed by the decompositional analysis.

The increased catalytic efficiency observed for cUNG when compared to hUNG is achieved through a combined effect resulting from increased k_{cat} and decreased K_m. While only the ground state of the chemical reaction catalyzed by UNG has been studied here, it would certainly be interesting to investigate the source of the increased k_{cat}. This requires, however, application of even more sophisticated computational approaches, such as hybrid quantum mechanics/molecular mechanical methods, and is left for future studies.

Acknowledgements Finacial support from the Research Council of Norway is gratefully acknowledged. The Norwegian Structural Biology Centre is supported by the Functional Genomics Program (FUGE) of the Research Council of Norway.

References

1. Hochachka PW, Somero GN (1984) Temperature adaptation, in Biochemical adaptations. Princeton University Press, Princeton, NJ, pp 355–449
2. Fields PA, Somero GN (1998) Proc Natl Acad Sci USA 95:11476–11481
3. Georlette D, Damien B, Blaise V, Depiereux E, Uversky VN, Gerday C, Feller G (2003) J Biol Chem 278:37015–37023
4. Leiros I, Moe E, Lanes O, Smalås AO, Willassen NP (2003) Acta Crystallogr D Biol Crystallogr 59:1357–1365
5. Olufsen M, Smalås AO, Moe E, Brandsdal BO (2005) J Biol Chem 280:18042–18048
6. Smalås AO, Heimstad ES, Hordvik A, Willassen NP, Male R (1994) Proteins 20:149–166
7. Brandsdal BO, Heimstad ES, Sylte I, Smalås AO (1999) J Biomol Struct Dyn 17:493–506
8. Russell RJM, Gerike U, Danson MJ, Hough DW, Taylor GL (1998) Structure 6:351–361
9. Kumar S, Nussinov R (2004) ChemBioChem 5:280–290
10. Gorfe AA, Brandsdal BO, Leiros HKS, Helland R, Smalås AO (2000) Proteins 40:207–217
11. Brandsdal BO, Smalås AO, Åqvist J (2001) FEBS Lett 499:171–175
12. Moe E, Leiros I, Riise EK, Olufsen M, Lanes O, Smalås A, Willassen NP (2004) J Mol Biol 343:1221–1230
13. Lindahl T, Nyberg B (1974) Biochemistry 13:3405–3410
14. Krokan HE, Standal R, Slupphaug G (1997) Biochem J 325:1–16
15. Mol CD, Arvai AS, Slupphaug G, Kavli B, Alseth I, Krokan HE, Tainer JA (1995) Cell 80:869–878
16. Savva R, Mcauleyhecht K, Brown T, Pearl L (1995) Nature 373:487–493
17. Ravishankar R, Sagar MB, Roy S, Purnapatre K, Handa P, Varshney U, Vijayan M (1998) Nucleic Acids Res 26:4880–4887
18. Geoui T, Buisson M, Tarbouriech N, Burmeister WP (2007) J Mol Biol 366:117–131
19. Bianchet MA, Seiple LA, Jiang YL, Ichikawa Y, Amzel LM, Stivers JT (2003) Biochemistry 42:12455–12460
20. Parikh SS, Mol CD, Slupphaug G, Bharati S, Krokan HE, Tainer JA (1998) EMBO J 17:5214–5226
21. Parikh SS, Walcher G, Jones GD, Slupphaug G, Krokan HE, Blackburn GM, Tainer JA (2000) Proc Natl Acad Sci USA 97:5083–5088
22. Slupphaug G, Mol CD, Kavli B, Arvai AS, Krokan HE, Tainer JA (1996) Nature 384:87–92
23. Lanes O, Leiros I, Smalås AO, Willassen NP (2002) Extremophiles 6:73–86
24. Dinner AR, Blackburn GM, Karplus M (2001) Nature 413:752–755
25. Pearlman DA, Case DA, Caldwell JW, Ross WS, Cheatham TE, Debolt S, Ferguson D, Seibel G, Kollman P (1995) Comput Phys Commun 91:1–41
26. Wang JM, Cieplak P, Kollman PA (2000) J Comput Chem 21:1049–1074
27. Jorgensen WL, Chandrasekhar J, Madura JD, Impey RW, Klein ML (1983) J Chem Phys 79:926–935
28. Berendsen HJC, Postma JPM, Vangunsteren WF, Dinola A, Haak JR (1984) J Chem Phys 81:3684–3690

29. Darden T, York D, Pedersen L (1993) J Chem Phys 98:10089–10092
30. Ryckaert JP, Ciccotti G, Berendsen HJC (1977) J Comput Phys 23:327–341
31. Kollman PA, Massova I, Reyes C, Kuhn B, Huo SH, Chong L, Lee M, Lee T, Duan Y, Wang W, Donini O, Cieplak P, Srinivasan J, Case DA, Cheatham TE (2000) Acc Chem Res 33:889–897
32. Massova I, Kollman PA (1999) J Am Chem Soc 121:8133–8143
33. Srinivasan J, Cheatham TE, Cieplak P, Kollman PA, Case DA (1998) J Am Chem Soc 120:9401–9409
34. Luo R, David L, Gilson MK (2002) J Comput Chem 23:1244–1253
35. Onufriev A, Bashford D, Case DA (2000) J Phys Chem B 104:3712–3720
36. Onufriev A, Bashford D, Case DA (2004) Proteins 55:383–394
37. Peter C, Oostenbrink C, van Dorp A, van Gunsteren WF (2004) J Chem Phys 120:2652–2661
38. Case DA (1994) Curr Opin Struc Biol 4:285–290
39. Karplus M, Kushick JN (1981) Macromolecules 14:325–332
40. Schafer H, Daura X, Mark AE, van Gunsteren WF (2001) Proteins 43:45–56
41. Schafer H, Mark AE, van Gunsteren WF (2000) J Chem Phys 113:7809–7817
42. Kuhn B, Kollman PA (2000) J Med Chem 43:3786–3791
43. Jayaram B, Sprous D, Beveridge DL (1998) J Phys Chem B 102:9571–9576
44. Connolly ML (1983) J Appl Cryst 16:548–558
45. Weiser J, Shenkin PS, Still WC (1999) J Comput Chem 20:217–230
46. Rocchia W, Alexov E, Honig B (2001) J Phys Chem B 105:6507–6514
47. Rocchia W, Sridharan S, Nicholls A, Alexov E, Chiabrera A, Honig B (2002) J Comput Chem 23:128–137
48. Moreira IS, Fernandes PA, Ramos MJ (2005) J Mol Struc Theochem 729:11–18
49. Jiang YL, Ichikawa Y, Song F, Stivers JT (2003) Biochemistry 42:1922–1929
50. Fersht A (1999) Structure and mechanism in protein science. In: Hadler GL (ed) W.H. Freeman and Company, NY
51. Brigo A, Lee KW, Fogolari F, Mustata GL, Briggs JM (2005) Proteins 59:723–741
52. Kuhn B, Kollman PA (2000) J Am Chem Soc 122:3909–3916
53. Adekoya OA, Willassen NP, Sylte I (2005) J Biomol Struct Dyn 22:521–531
54. Luo C, Xu LF, Zheng SX, Luo Z, Jiang XM, Shen JH, Jiang HL, Liu XF, Zhou MD (2005) Proteins 59:742–756
55. Wang W, Kollman PA (2000) J Mol Biol 303:567–582
56. Reyes CM, Kollman PA (2000) J Mol Biol 297:1145–1158
57. Zhang Q, Schlick T (2006) Biophys J 90:1865–1877
58. Gohlke H, Case DA (2004) J Comput Chem 25:238–250
59. Cao CY, Jiang YL, Stivers JT, Song FH (2004) Nat Struct Mol Biol 11:1230–1236
60. Parker CN, Halford SE (1991) Cell 66:781–791
61. Pearl LH (2000) Mut Res 460:165–181
62. Krosky DJ, Song FH, Stivers JT (2005) Biochemistry 44:5949–5959
63. Cao CY, Jiang YL, Krosky DJ, Stivers JT (2006) J Am Chem Soc 128:13034–13035
64. Jiang YL, Drohat AC, Ichikawa Y, Stivers JT (2002) J Biol Chem 277:15385–15392
65. Mol CD, Arvai AS, Sanderson RJ, Slupphaug G, Kavli B, Krokan HE, Mosbaugh DW, Tainer JA (1995) Cell 82:701–708
66. Wong I, Lundquist AJ, Bernards AS, Mosbaugh DW (2002) J Biol Chem 277:19424–19432
67. Chen CY, Mosbaugh DW, Bennett SE (2005) DNA Repair 4:793–805
68. Jiang YL, Kwon K, Stivers JT (2001) J Biol Chem 276:42347–42354
69. Stivers JT, Pankiewicz KW, Watanabe KA (1999) Biochemistry 38:952–963
70. DeLano WL (2002) The pyMol molecular graphics system. DeLano Scientific, San Carlos, CA, USA